ACS Catalysis

pubs.acs.org/acscatalysis Letter

Product Control in Visible-Light-Driven CO_2 Reduction by Switching Metal Centers of Binuclear Catalysts

Chao Su,[+] Hai-Hua Huang,[+] Zubing Huang,[+] Zilu Chen,* Anna Mo, Jia-Wei Wang, Huancheng Hu, Huahong Zou, Zhuofeng Ke, Fupei Liang,* Tong-Bu Lu,* and Dongcheng Liu*

Cite This: *ACS Catal.* 2025, 15, 2522−2530 Read Online

ABSTRACT: Controlled selectivity of products for visible-light-driven photocatalytic reduction of CO_2 in water-containing systems is highly desirable. Here, we report two highly efficient and selective binuclear complex catalysts, $[Co_2(^{Me}L\text{-}S)(OAc)_2](OAc)$ (**CoCo**) and $[Cu_2(^{Me}L\text{-}S)(H_2O)](CF_3SO_3)_2{\cdot}2H_2O$ (**CuCu**), bearing a N_6S-type polypyridine sulfur ligand ($^{Me}L\text{-}S^-$) in situ formed from 2,6-bis[(bis(pyridylmethyl)-amino)methyl]-4-methylmercaptophenylsulfide ($^{Me}L\text{-}S\text{-}S\text{-}L^{Me}$), which can promote the selective reduction of CO_2 into CO and HCOOH employing $[Ru(phen)_3](PF_6)_2$ as photosensitizer, respectively, under the irradiation of visible light in CH_3CN/H_2O (4/1 v/v) solution. We found that **CoCo** can catalyze the conversion of CO_2 to CO with a high selectivity (96%) and a TON value of 6188. However, HCOOH was found for the **CuCu** case with a high selectivity (98%) and TON value (7540). Experimental results and DFT calculations revealed that the close Cu···Cu distance in **CuCu** facilitates the hydrogenation process through a 3-center-4-electron (3c-4e$^-$) bond to give high efficiency and high HCOOH selectivity. However, 3c-4e$^-$ is absent in **CoCo** due to the well-separated Co centers and high total valence of the Co atoms, which lead to a high CO selectivity.

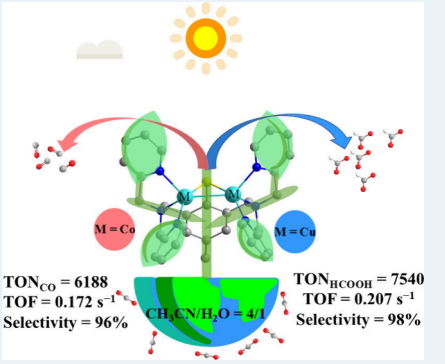

KEYWORDS: *photocatalytic CO_2 reduction, homogeneous, non-noble metal complex, visible-light, high efficiency and selectivity*

■ INTRODUCTION

The sunlight-driven reduction of CO_2 into fuels is a highly energy-demanding process and also a promising and sustainable path to mitigate anthropogenic CO_2 emissions.[1] However, its practical application is greatly limited due to poor product selectivity and low activity. Developing appropriate catalysts for photocatalytic CO_2 reduction is essential to realize carbon neutrality. Transition metal complexes as homogeneous molecular catalysts are suitable candidates which are valuable in elucidating structure−activity relationship and mechanism owing to the easy and precise adjustment of the ligand structures achieved through tuning electronic and spatial effects.[2] Recently, various metal complexes based on Re, Ru, Ir, Rh, Os, Cu, Co, Ni, Mn, and Fe have been developed for photocatalytic reduction of CO_2 reduction.[3] Although significant progress has been achieved over the recent decades, this promising technique still confronts with the following issues: (1) the product selectivity needs to be improved, especially in water-containing systems due to the competitive proton reduction reaction;[4] (2) visible-light-driven photocatalytic systems for CO_2 reduction always suffer from low efficiency;[5] (3) high capital expense for the catalyst was a limiting factor.[6] These issues significantly affect the feasibility and application of photochemical CO_2 reduction.[7]

Numerous attempts have been made to address the problems mentioned above in recent years. Modulating redox potentials of metal active centers through coordination sphere with ligand modifications is one of the effective ways to develop highly efficient and selective non-noble metal complex catalysts for CO_2 reduction.[8] For instance, systematic changes in the N-heterocyclic carbene-amine ligands have been surveyed through ligand modification by Chang and co-workers.[9] They found that the Ni complex supported by N-heterocyclic carbene-isoquinoline with extended conjugation reached a TON value of 98,000 in the visible-light-driven catalytic generation of CO from CO_2 in CH_3CN solution. Two mononuclear Fe(III) and Co(II) complexes constructed of a N_5-macrocycle ligand display product selectivity with a dependence on the metal centers of catalysts in the photoinduced reduction of CO_2 in CH_3CN solution. The photocatalytic system using the Co(II) complex gave a CO product with a high selectivity of 97% (TON = 270), while the same catalytic system employing the Fe(III) complex mainly produced HCOOH (TON = 5).[10] In 2019, the authors further reported a binuclear complex $[Co_2biqpy]^{4+}$ (biqpy =

Received: August 11, 2024
Revised: January 23, 2025
Accepted: January 24, 2025

https://doi.org/10.1021/acscatal.4c04800
ACS Catal. 2025, 15, 2522−2530

biquaterpyridine), which can selectively photoreduce CO_2 into HCOOH with a selectivity of 75.9% (TON = 821) in basic CH_3CN solution and to CO with a high selectivity of 96% (TON = 829) when phenol was used as a cosubstrate.[2b] However, most of the reported complexes with high selectivity and activity in photoreduction of CO_2 were achieved in pure organic solvent systems.[11]

We have recently developed two hydroxy-bridged binuclear cobalt complexes $[Co_2(L^1)(OAc)_2](OAc)$ and $[Co_2(L^2)(OAc)_2](OAc)$ supported by N_6O-type polypyridine ligands as efficient catalysts for cooperative conversion of CO_2 to CO under visible light irradiation in a water-containing system (Figure S1).[12] On the basis of the above complexes, we investigated the catalytic performance of binuclear copper complexes by changing the metal centers. Unfortunately, these copper complexes were not active in converting CO_2 to CO/HCOOH. On the other hand, HCOOH has also been found in other homogeneous photocatalytic systems employing polypyridine Mn, Fe, and Co complexes,[3k,8b,13] but the selectivity and/or HCOOH yield were very low.[2b] Inspired by efficient and selective metalloenzymes in nature, such as CO-dehydrogenase (CODH) and formate dehydrogenase (FDH), in which metal centers as the active sites are ligated by S atoms, complexes with coordination S atoms are potentially efficient and selective catalysts for photocatalytic CO_2 reduction. The coordination of S atoms can stabilize low-valent metal species considered as key intermediates in CO_2 reduction.[14] Combined with our previous work,[12,15] we are devoted to designing sulfur-bridging non-noble metal-based bimetallic complexes as catalysts for cooperative photocatalytic CO_2 reduction. Up to now, only a few examples of mononuclear nickel−sulfur complex have been explored as efficient molecular catalysts for photocatalytic and electrocatalytic CO_2 reduction,[14a,16] while there are no reports on multimetallic sulfur complexes employed as catalysts for homogeneous photocatalytic reduction of CO_2.

Herein, two binuclear metal−sulfur complexes of $[Co_2(^{Me}L\text{-}S)(OAc)_2](OAc)$ (**CoCo**) and $[Cu_2(^{Me}L\text{-}S)(H_2O)](CF_3SO_3)_2{\cdot}2H_2O$ (**CuCu**) were designed and employed as molecular catalysts bearing a bioinspired ligand for highly efficient and selective visible-light-driven CO_2 reduction in a water-containing (CH_3CN/H_2O, 4/1 v/v) system.[1d] It was found that CO was produced under visible light irradiation using cobalt complex catalyst **CoCo** with high TON_{CO} (6188) and excellent selectivity (96%) which are higher than those of most previously reported non-noble metal complex catalysts (Table S9), while HCOOH was formed (over 98%) using the copper-based catalyst **CuCu** with a TON_{HCOOH} value of 7540 (Table S10), demonstrating that the CO_2 reduction products can be switched through tuning metal centers of the catalysts. The present work opens new opportunities to develop molecular catalysts for highly efficient and selective visible-light-driven photocatalytic reduction of CO_2 into exclusively valuable products in aqueous solution.

■ METHODS AND MATERIALS

The binuclear complexes **CoCo** and **CuCu** were synthesized according to a reported procedure and characterized through single crystal X-ray diffraction, ESI-MS, XPS, and EPR analysis (Figure 1 and Figure S2). Based on the observations of ESI-MS for **CoCo**, the peak at m/z 813.1299 can be attributed to the species $\{[Co_2(^{Me}L\text{-}S)(OAc)_2] + CH_3OH\}^+$ (Figure S3). The valences of Co(II) in **CoCo** was confirmed by XPS

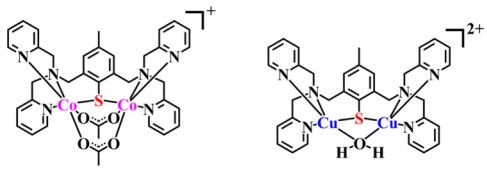

Figure 1. Structures of **CoCo** (left) and **CuCu** (right).

(Figure S4). The single crystal X-ray diffraction results indicated that **CuCu** crystallizes in the $P2_1/n$ space group and contains two Cu ions, one ligand $(^{Me}L\text{-}S)^-$, one μ_2-H_2O molecule, two $CF_3SO_3^-$ and two free H_2O molecules in the asymmetric unit. Crystallographic parameters (Table S1) and bond lengths and angles (Table S2) of **CuCu** are compiled in the Supporting Information. Cu1 and Cu2 are coordinated by one S atom and three N atoms from $(^{Me}L\text{-}S)^-$ and one μ_2-H_2O, forming a square pyramidal coordination geometry around the Cu atom (Figure 1 and Figure S2, Table S5).

CuCu was synthesized according to literature[17] which reported a mixed-valence binuclear complex $\mathbf{Cu^{1.5}Cu^{1.5}}$ with a Cu−Cu bond (2.5762(13) Å) and a highly delocalized mixed-valence state of $\mathbf{Cu^{+1.5}Cu^{+1.5}}$. However, the two Cu ions in **CuCu** are bridged by a H_2O with a longer Cu···Cu distance (2.8976(3) Å) than that in $\mathbf{Cu^{1.5}Cu^{1.5}}$, which might indicate different delocalized states of the two Cu ions in **CuCu**. On this basis, ESI-MS was first employed to verify the valence states of two Cu ions in **CuCu**. The main peaks m/z = 365.0582 and m/z = 879.0637 are assigned to $\{[Cu_2(^{Me}L\text{-}S)(H_2O)]^{2+} + CH_3CN\}$ and $\{[Cu_2(^{Me}L\text{-}S)(H_2O)]^{2+} + CF_3SO_3^- + CH_3CN\}$, respectively, which agree well with those simulated species based on their structural data (Figure S5). These results showed that the total number of valence states of the two Cu ions in **CuCu** was +3, indicating that **CuCu** is a mixed-valence complex. To further confirm whether **CuCu** exhibits equivalent or inequivalent copper centers, we investigated the metal valence in **CuCu** by XPS. The results showed that four main peaks and four satellite peaks appeared (Figure S4). The main peaks at 932.38 eV ($2P_{3/2}$) and 952.18 eV ($2P_{1/2}$) with satellite peaks at 941.28 eV ($2P_{3/2}$) and 961.48 eV ($2P_{1/2}$), respectively, reveal the presence of Cu^+.[18] Besides, the main peaks $2P_{3/2}$ = 934.08 eV and $2P_{1/2}$ = 954.08 eV with satellite peaks $2P_{3/2}$ = 934.28 eV and $2P_{1/2}$ = 962.88 eV reveal the presence of Cu^{2+}. These observations indicate that Cu^+ and Cu^{2+} simultaneously exist in **CuCu**.

Furthermore, to investigate the degree and potential reliance of spin localization on temperature, the electronic structure of **CuCu** was directly investigated by using variable-temperature EPR spectroscopy. The EPR spectrum of a frozen sample of **CuCu** in acetone/toluene (1:1 v/v) at temperatures between 77 and 170 K displayed four distinct peaks (Figure S6), which demonstrates that the unpaired electron spins ($S = {}^1/_2$) is predominantly found on Cu(II) ion (nuclear spin $I = {}^3/_2$) in **CuCu**. The experimental EPR spectrum of **CuCu** at 77 K was excellently fitted through a spectral simulation. (Figure 2). The hyperfine parameters used in the numerical simulation are in line with those for reported dicopper complexes.[19] At a temperature of 215 K, the four peaks in the EPR spectrum of **CuCu** (Figure S6) merged into a single resonance observed from 77 to 170 K.

However, the recorded spectrum of **CuCu** displayed seven peaks at 200 K compared to the spectrum with four peaks at 77 K (Figures S6 and S7). The extra hyperfine pattern at 200 K indicates that the unpaired electron spin shows partial

https://doi.org/10.1021/acscatal.4c04800
ACS Catal. 2025, 15, 2522−2530

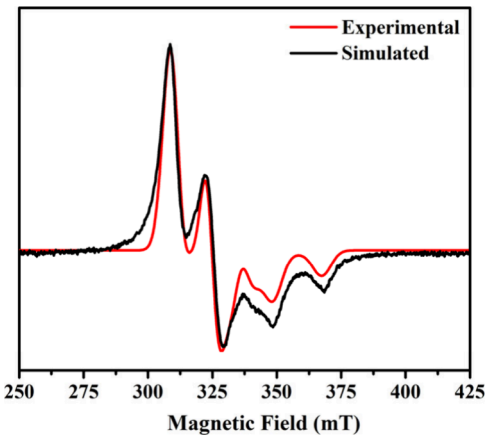

Figure 2. Simulated (red line) and experimental (black line) cw EPR spectra in toluene/acetone (1:1 v/v, 0.5 mM) for **CuCu** at 77 K with simulation results of g_1 = 2.032, g_2 = 2.096, g_3 = 2.165 and principal hyperfine components of A_1^{Cu} = 192, A_2^{Cu} = 66, A_3^{Cu} = 3 × 10^{-3} T.

delocalization over the two metal centers in **CuCu**. These results indicate that **CuCu** exhibits a temperature-dependent EPR spectrum with four peaks at low-temperature and increased hyperfine structure at relatively higher temperatures, consistent with previously reported dicopper Class II Cu(I)−Cu(II) complexes.[19a]

Photocatalytic experiments were first performed using **CuCu** and **CoCo** as catalysts with a photosensitizer of $[Ru(phen)_3](PF_6)_2$ (**Ru-PS**) and a sacrificial electron donor of TEOA in 5 mL of CH_3CN/H_2O (4/1 v/v) saturated with CO_2 under LED light (450 nm) irradiation (Table 1). It is noteworthy that **CuCu** (1 μM) afforded 2.34 μmol of HCOOH as the major product with trace amounts of H_2, while **CoCo** (1 μM) afforded 6.00 μmol of CO as the major product rather than HCOOH. The obtained corresponding TON_{HCOOH} and TON_{CO} values of **CuCu** and **CoCo** were 468 and 1200 with HCOOH and CO selectivities of 99% and 95%, respectively. These results showed that the reduction products of CO_2 can be switched by changing the metal centers of the complex catalysts.

Several sacrificial electron donors have been utilized to optimize the photocatalytic system when **CuCu** and **CoCo** (1.0 μM) were used as catalysts (Table 1, Entries 3−6). We conducted a preliminary exploration of **CoCo** and **CuCu** for photocatalytic CO_2 reduction systems using TEOA and TEA. Significantly, **CuCu** is more efficient when TEA was used as a sacrificial reductant compared to TEOA (Table 1, Entries 1 and 3), producing 10.51 μmol of HCOOH with a TON_{HCOOH} value of 2102 and a selectivity of 98% (Figure 3). In sharp

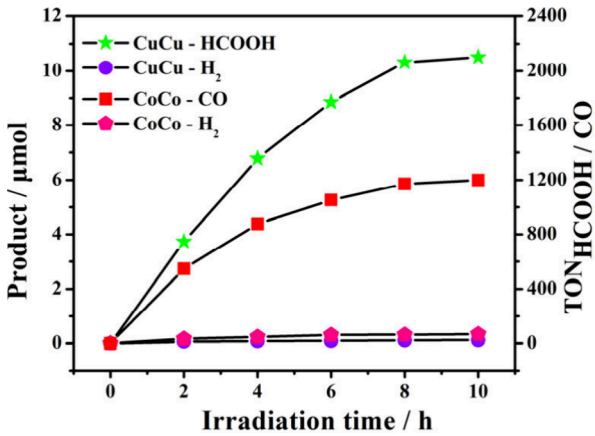

Figure 3. Time-dependent photocatalytic evolution of HCOOH/CO and H_2 within 10 h in the presence of **CuCu**/**CoCo** (1 μM), sacrificial reductant (0.3 M, TEA for **CuCu** and TEOA for **CoCo**), and **Ru-PS** (0.4 mM) in a CO_2-saturated CH_3CN/H_2O (4/1 v/v) under 450 nm LED light irradiation.

contrast, **CoCo** only produced 1.67 μmol of CO with a smaller TON_{CO} value (333) and a lower selectivity (64%) employing the sacrificial reductant of TEA compared to TEOA (Table 1, Entries 2 and 6). In addition, the catalytic efficiency of the system catalyzed by **CuCu** cannot be improved when the sacrificial reductant TEOA was replaced by 1-benzyl-4*H*-pyridine-3-carboxamide (BINH) (Table 1, Entry 4). On the other hand, the catalytic system in 5 mL of water using **CuCu** as a catalyst, L-ascorbic acid sodium (VCNa) as sacrificial reductant, and $[Ru(bpy)_3]Cl_2$ as photosensitizer (Table 1, Entry 5) shows photocatalytic reduction of CO_2 to HCOOH giving a maximum TON_{HCOOH} (310) and HCOOH selectivity (76%) values until now among systems catalyzed by non-noble metal complex catalysts in an aqueous solution.[20] These results suggested that TEA (0.3 M), **Ru-PS** (0.4 mM), and CH_3CN/H_2O (4/1 v/v 5 mL) are optimal for CO_2-to-HCOOH conversion catalyzed by **CuCu**, but TEOA is superior to TEA when **CoCo** is used in photocatalytic reduction of CO_2 to CO. The catalytic systems with TEA as sacrificial electron donor show relatively stronger alkaline than that of TEOA, which is favorable to stabilize the hydrogenation species $[Cu^{III}Cu^{I}(L^-)(H^-)]^{2+}$ for photocatalytic reduction of CO_2 to HCOOH employing **CuCu** as catalyst. However, the catalytic systems for

Table 1. Photoinduced Reduction of CO_2 by CuCu and CoCo in Different Conditions[a]

Entry	Cat.	PS	SD	HCOOH [μmol]	CO [μmol]	H_2 [μmol]	HCOOH/CO [%]	TON	TOF [s^{-1}]
1	CuCu	Ru-PS	TEOA	2.34	0	0.015	99	468	0.013
2	CoCo	Ru-PS	TEOA	0	6.00	0.336	95	1200	0.033
3	CuCu	Ru-PS	TEA	10.51	0	0.202	98	2102	0.058
4	CuCu	Ru-PS	BINH	2.90	0	0.29	91	580	0.016
5	CuCu	$[Ru(bpy)_3]Cl_2$	VCNa	1.55	0	0.5	76	310	0.009
6	CoCo	Ru-PS	TEA	0	1.67	0.955	64	333	0.009
7	CoCo	Ru-PS	TEOA	0	1.55	0.064	96	6188	0.172
8	Co	Ru-PS	TEOA	0	3.92	0.38	91	390	0.011

[a]Reaction conditions: a mixed solution CH_3CN/H_2O (5 mL 4/1 v/v) containing **CuCu**/**CoCo** (1 μM); BINH/VCNa (20 mg) or TEA/TEOA (0.3 M), **Ru-PS** (0.4 mM) illumination for 10 h with a 450 nm LED light (irradiation area 0.8 cm^2, 100 mW·cm^{-2}). Entry 5: H_2O (5 mL). Entry 7: **CoCo** (0.05 μM). Entry 8: **Co** (2 μM). The values are averaged over three photocatalytic tests with deviations below 10%.

https://doi.org/10.1021/acscatal.4c04800
ACS Catal. 2025, 15, 2522−2530

photocatalytic CO_2 reduction to CO using **CoCo** as catalyst is more efficient in relatively weaker alkaline solution with TEOA as sacrificial reductant.[21]

To conduct an in-depth assessment of this water-based photocatalytic system for CO_2 reduction, a series of control experiments were conducted employing **CuCu** as a representative example. With the absence of **CuCu**, no HCOOH was observed in the catalytic system, which suggested that the produced HCOOH stem from CO_2 reduction catalyzed by **CuCu**. (Table S3, Entry 4). Besides, the further control experiments without sacrificial reductant, light, **Ru-PS**, or CO_2, and control experiments with $[Cu(CF_3SO_3)(CH_3CN)_4]$, $(Co(CH_3COO)_2{\cdot}4H_2O$, or ligand ^{Me}L-S-S-L^{Me} led to no appreciable HCOOH formation (Table S3, Entries 2, 3, 5, 6, 7,10, and 11). In addition, $^{13}CO_2$ isotope trace experiments were conducted to verify the carbon source of HCOOH/CO. As shown in Figures S8, the ^{13}C NMR spectrum shows the $H^{13}COO^-$ signal at 170 ppm, confirming that $HCOO^-$ originates from CO_2. The peak at m/z = 29 in the mass spectrum (MS), can be ascribed to ^{13}CO, confirming that CO_2 was the source of CO.[22]

The outcomes of these experiments confirm the essential roles of the catalyst, sacrificial reductant, photosensitizer, visible-light, and CO_2 in the functioning of this photocatalytic system. Moreover, CO_2 can be effectively reduced in this water-containing photocatalytic system even under simulated flue conditions (10% CO_2 atmosphere) (Table S3, Entry 7) with a TON_{HCOOH} of 464 and a HCOOH selectivity of 80% which are even higher than those of reported non-noble metal complexes for photocatalytic CO_2-to-HCOOH conversion in pure CO_2.[13a,23] The photocatalytic performance of the system after addition of Hg^0 (Table S3, Entry 8), indicating that the molecular catalyst is responsible for the generation of HCOOH. Under the same conditions, the correlation between the HCOOH evolution and catalyst concentration was examined (Table S4). We evaluated the performance of photocatalytic systems under different **CuCu** concentrations. 23.95 μmol of HCOOH was obtained when the concentration of **CuCu** was raised to 10 μM, exhibiting a HCOOH selectivity as high as 99% (Table S4, Entry 1). Upon decreasing the concentration of **CuCu** to 0.1 μM, 3.77 μmol of HCOOH was detected$_2$, leading to the TON value of HCOOH up to 7540 (Table S4, Entry 3), respectively.[8a,24,16a] **CuCu** is a competent copper-based molecular catalyst for photochemical CO_2-to-HCOOH conversion.[8d]

The durability of **CuCu** and **CoCo** was also examined in this photocatalytic system for the reduction of CO_2 (Figure S9). It was found that the absorbance of complexes **CoCo** and **CuCu** display no obvious alterations pre and post 10 h irradiation, indicating that **CoCo** and **CuCu** are stable in the solution under irradiation. The discontinuation of the photocatalytic reaction for CO_2 reduction is possibly due to the degradation of catalyst **CuCu**/**CoCo** and/or photosensitizer **Ru-PS** because sacrificial reductant (TEA/TEOA) is in large excess in the catalytic system. The absorbance of **Ru-PS** showed an apparent decrease when exposed to visible light irradiation for 10 h (Figure S10). Then, the degradation of **Ru-PS** was verified by electrospray mass spectrometry (ESI-MS) (Figure S11).[12b] The intensity of the peak at m/z 312.05 of $[Ru(phen)_3]^{2+}$ gradually decreased with visible light illumination. Based on experimental evidence, it was reasoned that the inactivation of the CO_2 reduction process can be due to the instability of photosensitizer **Ru-PS**. To verify our conjecture, consecutive experiments were conducted. Noticeably, the photocatalytic reduction of CO_2 into HCOOH/CO was restarted by introducing fresh photosensitizer **Ru-PS** (0.4 mM) (Figure S10 and Figure S11). However, the reaction with fresh sacrificial reductants (TEA/TEOA) or catalyst (**CoCo**) cannot be reactivated (Figures S12−S14). These findings, combined with mercury poisoning experiments (Table S3, Entry 9) and the dynamic light scattering (DLS) experiments (Figure S15), indicated that **CoCo** and **CuCu** are highly stable homogeneous molecular catalysts. It was found that HCOOH production catalyzed by **CuCu** (1 μM) showed a good linear relationship with time within 2 h (Figure S16). Furthermore, experiments showed that the production of HCOOH show a first-order liner dependence on the concentration of **CuCu** in the first 2 h (Figure S17), which reveals that the rate-limiting step involves a single Cu site in the photoinduced CO_2 reduction process.

Besides, we synthesized a mononuclear complex $[CoN_3S]$-ClO_4 (**Co**) (L = (*N*,*N*-bis(2-pyridylmethyl)-*N*-(2-benzylthiol)amine, Figure S18)[4b] to comfirm that two complexes **CoCo**/**CuCu** show synergistic catalysis for photoinduced CO_2 reduction as our reported work.[12] Similar experiments of visible-light driven reduction of CO_2 to CO was performed for **Co** using **Co** (2.0 μM) instead of **CoCo** (1.0 μM) to maintain the same concentration of Co^{II} ion. Obviously, **Co** has a certain activity (TON_{CO}, 390; selectivity, 91%) for photocatalytic conversion of CO_2-to-CO (Table 1, Entry 8). These values are much smaller than those of binuclear complex **CoCo** (Table 1, Entry 2; TON_{CO}, 1200; selectivity, 95%). The TON_{CO} values demonstrated that two Co^{II} ions within **CoCo** probably show a synergistic catalysis effect, which endows **CoCo** with high CO_2-to-CO catalytic activity.

For exploring the photocatalytic-structural correlations of **CoCo**/**CuCu**, their electrochemical behaviors were investigated through DPV (differential pulse voltage) and CV (cyclic voltammetry). Under a N_2 atmosphere, the CV of **CoCo** exhibits an irreversible reductive process at −1.00 V vs NHE determined to be $Co^{II}Co^{II}/Co^{II}Co^{I}$ (Figures S19 and S20). The redox potentials of metal centers in **CuCu** cannot be obtained via CV of **CuCu** (Figure S19). The DPV of **CuCu** shows three reductive processes as shown in Figure S20. Under a N_2 atmosphere, the CV of ligand ^{Me}L-S-S-L^{Me} exhibits a reductive process at −0.48 V vs NHE (Figure S19). Therefore, the peaks at −0.31 V vs NHE and −1.09 V vs NHE in the DPV of **CuCu** can be assigned to $Cu^{II}Cu^{II}/Cu^{II}Cu^{I}$ and $Cu^{II}Cu^{I}/Cu^{I}Cu^{I}$, respectively, which are in line with the results of theoretical calculations. Under a CO_2 atmosphere, the current increase obviously in the CVs of **CoCo** and **CuCu**, suggesting electrocatalysis for CO_2 reduction. Besides, the onset potentials of electrocatalytic current are −0.72 and −0.79 V vs NHE for **CoCo** and **CuCu**, respectively, which are more positive potentials than the redox potential (−0.84 V vs NHE) of $[\mathbf{Ru\text{-}PS}]^{3+/2+*}$, indicating a thermodynamically feasible electron transfer from **Ru-PS*** to **CuCu**/**CoCo** in our photocatalytic system. It agrees well with the catalytic performance of **CoCo** and **CuCu** for photochemical CO_2 reduction. Besides, based on the experiment results for the addition of water as shown in Figure S21, the CV curves of **CoCo** shift to more positive potentials and the current density increases obviously.[25] At the same time, the influence of CH_3COONa was investigated via an electrochemical test. The increasing CH_3COONa concentrations could retain the

https://doi.org/10.1021/acscatal.4c04800
ACS Catal. 2025, 15, 2522−2530

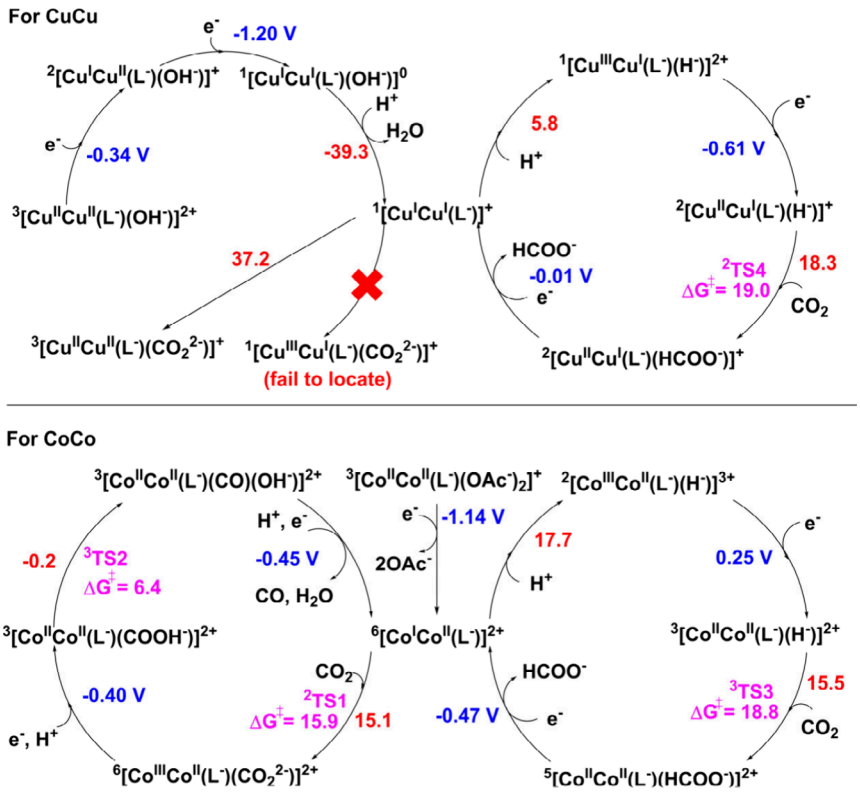

Figure 4. Proposed mechanisms for the visible-light-driven reduction of CO_2 to CO/HCOOH catalyzed by **CoCo** and **CuCu**. The free energy changes (red) and barriers (pink) are presented in kcal·mol^{-1}. The calculated potentials (blue) are presented in V vs NHE.

irreversible wave at this condition but still induce increasing currents, potentially from hydrogen evolution enhanced with acetic acid from the reaction of acetate with water. This implies the complicated acetate-dissociation processes involved in the redox events, while its possible pathways have been preliminarily revealed by our DFT results.

To further comprehend the mechanism for product control in the photochemical reduction of CO_2 by switching of the metal centers, we further investigated the pathway of electron delivery in this photocatalytic system. The fluorescence intensity of the excited state of photosensitizer **Ru-PS** shows no obviously change dependence on the increase of the concentration of sacrificial reductants TEA/TEOA (Figure S23). Nevertheless, photosensitizer **Ru-PS*** in the excited state was rapdly quenched by **CuCu** or **CoCo** giving apparent quenching rate constants of 6.54×10^9 M^{-1} S^{-1} and 6.31×10^9 M^{-1} S^{-1} according to the Stern−Volmer equation (Figure S24 and Figure S25). These observations indicated that the excited state photosensitizer can be efficiently quenched by **CuCu** and **CoCo** in the catalytic system following an oxidation quenching path.[9,12,26]

To demonstrate the formation of Cu−H bonds, we prepared metal hydrides by treating **CuCu** with 1 equimolar amounts of $NaBEt_3H$ in THF in glovebox (298 K) and characterized them using ^{1}H NMR. A peak at −0.8 ppm (Figure S26) was observed for the bridging hydride (yield: 15%) through referencing to those reported dinuclear copper complexes.[8d,27]

Density functional theory (DFT) calculations were also applied to investigate the catalytic mechanism and revealed the factors for the different selectivity. The optimum pathways for the photocatalytic CO_2 reduction were proposed in Figure 4. For the Co complex, we investigated the EPR of **CoCo** as shown in Figure S27. The strong signal peak at g = 2.21 indicates the presence of unpaired electrons in Co centers and without obvious electronic coupling between the two Co centers in **CoCo**. In addition, the free energy of **CoCo** at the open-shell antiferromagnetic singlet state was calculated to be slightly higher than that of the triplet species (Table S6 and Table S7). Therefore, the triplet state is more likely.[22a,28] The calculated potential for the first reduction step is −1.29 V. This value can be reduced to −1.14 V if the exergonic process of acetate departure is under consideration, which is close to the experimental value. After the formation of $[Co^{I}Co^{II}(L^{-})]^{2+}$, the pathway for the CO product and the pathway for the HCOOH product were studied, respectively. In the CO pathway, the barrier for the coordination of the CO_2 to $[Co^{I}Co^{II}(L^{-})]^{2+}$ was calculated to be 15.9 kcal/mol to generate $[Co^{III}Co^{II}(L^{-})(COO^{2-})]^{2+}$ (Figure S28−S30 and Table S6), which is lower than that for the pathway with one acetate anion (19.9 kcal/mol) probably due to the reduced steric hindrance after the departure of the acetate ligand (Table S8). In fact, the CO_2^{2-} ligand in $[Co^{III}Co^{II}(L^{-})(COO^{2-})]^{2+}$ is coordinated to just one center, probably due to the relatively low electron density of the partially reduced CO_2 moiety, which is also suggested by the O−C−O angle of 148.8°, as well as the C−O bond distances (1.23 and 1.21 Å, Figure S31). After a further PCET process, the formed $[Co^{II}Co^{II}(L^{-})(COOH^{-})]^{2+}$ intermediate exhibits a structure that the COOH moiety is bridging between the two cobalt centers, since the 2-e$^-$ reduction of CO_2 has been completed, as indicated by the O−C−O angle of 112.8° and the higher C−O(H) distance of 1.48 Å. Subsequently, C−O cleavage of $[Co^{II}Co^{II}(L^{-})(COOH^{-})]^{2+}$ with a barrier of 6.4 kcal/mol gave $[Co^{II}Co^{II}(L^{-})(CO)(OH^{-})]^{2+}$ (Figure 4 and Figure S32),

https://doi.org/10.1021/acscatal.4c04800
ACS Catal. 2025, 15, 2522−2530

which was converted back into the $[Co^{I}Co^{II}(L^{-})]^{2+}$ accompanied with the release of CO and H_2O after a further PCET process. The CO_2 coordination step is likely to be rate-determining, which has a total free energy barrier of 22.9 kcal/mol with consideration of the formation energy of $[Co^{I}Co^{II}(L^{-})]^{2+}$ (Figure S32).

In the HCOOH pathway, the hydrogenation of $[Co^{I}Co^{II}(L^{-})]^{2+}$ gave $[Co^{III}Co^{II}(L^{-})(H^{-})]^{3+}$ with a free energy change of 17.7 kcal/mol (Figure 4 and Figure S32), followed by a reduction step to generate $[Co^{II}Co^{II}(L^{-})(H^{-})]^{2+}$. Then the CO_2 insertion step required a barrier of 18.8 kcal/mol and $[Co^{II}Co^{II}(L^{-})(HCOO^{-})]^{2+}$ was formed. After a further electron transfer step accompanied by the departure of $HCOO^{-}$, $[Co^{I}Co^{II}(L^{-})]^{2+}$ was regenerated to close the catalytic cycle. If the formation energy of $[Co^{I}Co^{II}(L^{-})]^{2+}$ is considered, the rate-limiting step might be the hydrogenation of $[Co^{I}Co^{II}(L^{-})]^{2+}$ with a total free energy change of 24.7 kcal/mol (Figure S32). Therefore, the HCOOH pathway seems to be less favored compared with the CO pathway since the latter one exhibits a lower rate-determining barrier (22.9 kcal/mol), consistent with the high CO selectivity.

In terms of the Cu complex, the low valence center Cu(I) in **CuCu** was oxidized to Cu(II) in the alkaline reaction solution, and H_2O was replaced by OH^{-} to give $[Cu^{II}Cu^{II}(L^{-})(OH^{-})]^{+}$, which was confirmed by ESI-MS spectra (Figure S33). Two-steps 1-e^{-} reduction of $[Cu^{II}Cu^{II}(L^{-})(OH^{-})]^{+}$ gave $[Cu^{I}Cu^{I}(L^{-})(OH^{-})]$ (Figure 4). The potentials of $Cu^{II}Cu^{II}/Cu^{II}Cu^{I}$ and $Cu^{II}Cu^{I}/Cu^{I}Cu^{I}$ were calculated to be −0.34 and −1.20 V, which are consistent with experimental results. The closed-shell singlet $[Cu^{I}Cu^{I}(L^{-})]^{+}$ was formed after the protonation of the hydroxyl group and the departure of water, but the direct coordination of CO_2 to the closed-shell singlet species was failed. Although the structure of the open-shell triplet $[Cu^{II}Cu^{II}(L^{-})(COO^{2-})]^{+}$ was optimized successfully, an extremely high free energy change of 37.2 kcal/mol was obtained relative to that of the closed-shell singlet $[Cu^{I}Cu^{I}(L^{-})]^{+}$ (Figure 4 and Figure S34). The total barrier should be higher than that value, making it difficult to occur at room temperature.

The calculated free energy change for the hydrogenation of $[Cu^{I}Cu^{I}(L^{-})]$ to $[Cu^{III}Cu^{I}(L^{-})(H^{-})]^{2+}$ is only 5.8 kcal/mol (Figure 4). A subsequent 1-e^{-} reduction gave $[Cu^{II}Cu^{I}(L^{-})(H^{-})]^{+}$ with a calculated potential of −0.61 V, followed by a hydride insertion step with a barrier of 19.0 kcal/mol and $[Cu^{II}Cu^{I}(L^{-})(HCOO^{-})]^{+}$ was formed (Figure S30 and Figure S34). A further 1-e^{-} reduction accompanied with the departure of $HCOO^{-}$ regenerated $[Cu^{I}Cu^{I}(L^{-})]$ and closed the catalytic cycle. These results are consistent with the high HCOOH selectivity in photocatalysis.

The poor ability of Cu complex **CuCu** for CO_2 coordination is presumably partially attributed to steric hindrance caused by the close Cu···Cu distance (Figure S35), which is only 2.67 Å in singlet $[Cu^{I}Cu^{I}(L^{-})]^{+}$. This value increases to 3.38 Å in the CO_2 coordinating species triplet $[Cu^{II}Cu^{II}(L^{-})(COO^{2-})]^{+}$ (Figures S35−S36), indicating significant structural change. Contrarily, two Co atoms are well separated in the Co complex, and no significant change in the Co···Co distance is observed from $[Co^{I}Co^{II}(L^{-})]^{2+}$ (4.31 Å) to $[Co^{III}Co^{II}(L^{-})(COO^{2-})]^{2+}$ (4.07 Å) (Figure S35 and Figure S37).

With respect to the hydrogenation step, the steric hindrance seems to be insignificant owing to the extremely small size of the proton. Thanks to the close Cu···Cu distance, two Cu atoms are both involved in the hydrogenation process via a 3-center-4-electron (3c-4e^{-}) bond (Figure S38), stabilizing the formal Cu^{III} center in $[Cu^{III}Cu^{I}(L^{-})(H^{-})]^{2+}$. A similar 3c-4e^{-} bond is absent in the Co complex due to the well-separated Co centers and the higher total valence of the Co atoms than that of Cu atoms in **CuCu**, leading to lower proton affinity, consistent with the high formation energy of $[Co^{III}Co^{II}(L^{-})(H^{-})]^{3+}$ and the low HCOOH selectivity.

CONCLUSION

In conclusion, we have presented two binuclear Co and Cu complexes supported by a N_6S-type polypyridine sulfur ligand that can act as highly efficient and selective homogeneous molecular catalysts in water-containing systems for visible-light-driven reduction of CO_2 to HCOOH or CO by switching the catalytically active centers. CO is obtained in the case for Co complex, while the Cu analogue leads to clean formation of HCOOH under the same conditions. It was found that the close Cu···Cu distance in **CuCu** facilitates the hydrogenation process through a 3c-4e^{-} bond to give high performance for photocatalytic CO_2-to-HCOOH conversion. This work provides new insights for designing high-performance molecular catalysts for homogeneous catalytic CO_2 reduction.

ASSOCIATED CONTENT

Supporting Information

The Supporting Information is available free of charge at https://pubs.acs.org/doi/10.1021/acscatal.4c04800.

Preparative methods, spectral and analytical data, mechanistic investigations, and theoretical calculations, crystal data, bond lengths and angles, reduction data, tau values, free energies, structures, MS spectra, XPS profiles, EPR spectra, NMR spectra, UV−vis spectra, degradation trend, particle size distribution, time-product diagram, amounts of HCOOH evolution, CVs, DPV, emission intensity, free energy barriers, energy diagrams, molecular orbitals, coordinates (PDF)

AUTHOR INFORMATION

Corresponding Authors

Zilu Chen − *State Key Laboratory for Chemistry and Molecular Engineering of Medicinal Resources, School of Chemistry and Pharmaceutical Sciences, Guangxi Normal University, Guilin 541004, China;* orcid.org/0000-0003-1341-2330; Email: zlchen@mailbox.gxnu.edu.cn

Fupei Liang − *State Key Laboratory for Chemistry and Molecular Engineering of Medicinal Resources, School of Chemistry and Pharmaceutical Sciences, Guangxi Normal University, Guilin 541004, China;* orcid.org/0000-0001-7435-0140; Email: liangfupei@glut.edu.cn

Tong-Bu Lu − *International Joint Laboratory of Materials Microstructure, Institute for New Energy Materials and Low Carbon Technologies, School of Materials Science and Engineering, Tianjin University of Technology, Tianjin 300384, China;* orcid.org/0000-0002-6087-4880; Email: lutongbu@tjut.edu.cn

Dongcheng Liu − *State Key Laboratory for Chemistry and Molecular Engineering of Medicinal Resources, School of Chemistry and Pharmaceutical Sciences, Guangxi Normal University, Guilin 541004, China;* orcid.org/0000-0002-6420-5473; Email: ldcheng@mailbox.gxnu.edu.cn

https://doi.org/10.1021/acscatal.4c04800
ACS Catal. 2025, 15, 2522−2530

Authors

Chao Su − *State Key Laboratory for Chemistry and Molecular Engineering of Medicinal Resources, School of Chemistry and Pharmaceutical Sciences, Guangxi Normal University, Guilin 541004, China*

Hai-Hua Huang − *Key Lab of Fluorine and Silicon for Energy Materials and Chemistry of Ministry of Education, College of Chemistry and Materials, Jiangxi Normal University, Nanchang 330022, China*

Zubing Huang − *State Key Laboratory for Chemistry and Molecular Engineering of Medicinal Resources, School of Chemistry and Pharmaceutical Sciences, Guangxi Normal University, Guilin 541004, China*

Anna Mo − *State Key Laboratory for Chemistry and Molecular Engineering of Medicinal Resources, School of Chemistry and Pharmaceutical Sciences, Guangxi Normal University, Guilin 541004, China*

Jia-Wei Wang − *State Key Laboratory for Chemistry and Molecular Engineering of Medicinal Resources, School of Chemistry and Pharmaceutical Sciences, Guangxi Normal University, Guilin 541004, China;* orcid.org/0000-0003-1966-7131

Huancheng Hu − *State Key Laboratory for Chemistry and Molecular Engineering of Medicinal Resources, School of Chemistry and Pharmaceutical Sciences, Guangxi Normal University, Guilin 541004, China;* orcid.org/0000-0001-6521-5086

Huahong Zou − *State Key Laboratory for Chemistry and Molecular Engineering of Medicinal Resources, School of Chemistry and Pharmaceutical Sciences, Guangxi Normal University, Guilin 541004, China;* orcid.org/0000-0003-1759-3714

Zhuofeng Ke − *School of Materials Science & Engineering, PCFM Lab, School of Chemistry, Sun Yat-sen University, Guangzhou 510275, PR China;* orcid.org/0000-0001-9064-8051

Complete contact information is available at: https://pubs.acs.org/10.1021/acscatal.4c04800

Author Contributions

[+]Chao Su, Hai-Hua Huang and Zubing Huang contributed equally to this word.

Funding

The work was financially supported by the Guangxi Technology Base and Talent Subject (grant no. GUIKE AD23026067), the National Natural Science Foundation of China (Nos. 22061004, 22361005, 12064002, 22402070, and 22261007), the Science and Technology Planning Project of Guangzhou (202201011113) and the Guangdong Basic and Applied Basic Research Foundation (2022A1515110079).

Notes

The authors declare no competing financial interest.

ACKNOWLEDGMENTS

The work was financially supported by the Guangxi Technology Base and Talent Subject (grant no. GUIKE AD23026067), the National Natural Science Foundation of China (Nos. 22061004, 22361005, 12064002, 22402070 and 22261007), the Science and Technology Planning Project of Guangzhou (202201011113) and the Guangdong Basic and Applied Basic Research Foundation (2022A1515110079). Our gratitude goes to Prof. Zhaobo Hu for his excellent analytical and technical support in EPR.

ABBREVIATIONS

Ru-PS, $[Ru(phen)_3](PF_6)_2$

REFERENCES

(1) (a) Lei, Q.; Yuan, H.; Du, J.; Ming, M.; Yang, S.; Chen, Y.; Lei, J.; Han, Z. Photocatalytic CO_2 reduction with aminoanthraquinone organic dyes. *Nat. Commun.* **2023**, *14*, 1087. (b) Santiago, R.-J.; Song, H. W.; Lam, E.; Wright, D.; Pannwitz, A.; Bonke, S. A.; Baumberg, J. J.; Bonnet, S.; Hammarstrom, L.; Reisner, E. Self-Assembled Liposomes Enhance Electron Transfer for Efficient Photocatalytic CO_2 Reduction. *J. Am. Chem. Soc.* **2022**, *144*, 9399−9412. (c) Yuan, H.; Cheng, B.; Lei, J.; Jiang, L.; Han, Z. Promoting photocatalytic CO_2 reduction with a molecular copper purpurin chromophore. *Nat. Commun.* **2021**, *12*, 1835−1844. (d) Wang, H. F.; Wang, H. J.; Zhong, D. C.; Lu, T. B. Unveiling the role of proton concentration in dinuclear metal complexes for boosting photocatalytic CO_2 reduction. *Proc. Natl. Acad. Sci. U. S. A.* **2024**, *121*, No. e2318384121.

(2) (a) Zhang, B.; Sun, L. Artificial photosynthesis: opportunities and challenges of molecular catalysts. *Chem. Soc. Rev.* **2019**, *48*, 2216−2264. (b) Guo, Z.; Chen, G.; Cometto, C.; Ma, B.; Zhao, H.; Groizard, T.; Chen, L.; Fan, H.; Man, W.; Yiu, S. M.; Lau, K. C.; Lau, T. C.; Robert, M. Selectivity control of CO versus $HCOO^-$ production in the visible-light-driven catalytic reduction of CO_2 with two cooperative metal sites. *Nat. Catal.* **2019**, *2*, 801−808. (c) Yuan, H.; Krishna, A.; Wei, Z.; Su, Y.; Chen, J.; Hua, W.; Zheng, Z.; Song, D.; Mu, Q.; Pan, W.; Xiao, L.; Yan, J.; Li, G.; Yang, W.; Deng, Z.; Peng, Y. Ligand-Bound CO_2 as a Nonclassical Route toward Efficient Photocatalytic CO_2 Reduction with a Ni N-Confused Porphyrin. *J. Am. Chem. Soc.* **2024**, *146*, 10550−10558. (d) Ishizuka, T.; Hosokawa, A.; Kawanishi, T.; Kotani, H.; Zhi, Y.; Kojima, T. Self-Photosensitizing Dinuclear Ruthenium Catalyst for CO_2 Reduction to CO. *J. Am. Chem. Soc.* **2023**, *145*, 23196−23204. (e) Wang, J. W.; Jiang, L.; Huang, H. H.; Han, Z.; Ouyang, G. Rapid electron transfer via dynamic coordinative interaction boosts quantum efficiency for photocatalytic CO_2 reduction. *Nat. Commun.* **2021**, *12*, 4276.

(3) (a) Wang, J. W.; Jiang, L.; Huang, H. H.; Han, Z.; Ouyang, G. F. Rapid electron transfer via dynamic coordinative interaction boosts quantum efficiency for photocatalytic CO_2 reduction. *Nat. Commun.* **2021**, *12*, 4276−4287. (b) Ghosh, A. C.; Legrand, A.; Rajapaksha, R.; Craig, G. A.; Sassoye, C.; Balazs, G.; Farrusseng, D.; Furukawa, S.; Canivet, J.; Wisser, F. M. Rhodium-Based Metal-Organic Polyhedra Assemblies for Selective CO_2 Photoreduction. *J. Am. Chem. Soc.* **2022**, *144*, 3626−3636. (c) Tamaki, Y.; Morimoto, T.; Koike, K.; Ishitani, O. Photocatalytic CO_2 reduction with high turnover frequency and selectivity of formic acid formation using Ru(II) multinuclear complexes. *Proc. Natl. Acad. Sci. U.S.A.* **2012**, *109*, 15673−15678. (d) Kamada, K.; Jung, J.; Wakabayashi, T.; Sekizawa, K.; Sato, S.; Morikawa, T.; Fukuzumi, S.; Saito, S. Photocatalytic CO_2 Reduction Using a Robust Multifunctional Iridium Complex toward the Selective Formation of Formic Acid. *J. Am. Chem. Soc.* **2020**, *142*, 10261−10266. (e) Kothandaraman, J.; Goeppert, A.; Czaun, M.; Olah, G. A.; Prakash, G. K. Conversion of CO_2 from Air into Methanol Using a Polyamine and a Homogeneous Ruthenium Catalyst. *J. Am. Chem. Soc.* **2016**, *138*, 778−781. (f) Fabry, D. C.; Koizumi, H.; Ghosh, D.; Yamazaki, Y.; Takeda, H.; Tamaki, Y.; Ishitani, O. A Ru(II)−Mn(I) Supramolecular Photocatalyst for CO_2 Reduction. *Organometallics* **2020**, *39*, 1511−1518. (g) Rao, H.; Schmidt, L. C.; Bonin, J.; Robert, M. Visible-light-driven methane formation from CO_2 with a molecular iron catalyst. *Nature* **2017**, *548*, 74−77. (h) Guo, Z.; Yu, F.; Yang, Y.; Leung, C. F.; Ng, S. M.; Ko, C. C.; Cometto, C.; Lau, T. C.; Robert, M. Photocatalytic Conversion of CO_2 to CO by a Copper(II) Quaterpyridine Complex. *ChemSusChem* **2017**, *10*, 4009−4013. (i) Wang, J. W.; Liu, W. J.; Zhong, D. C.; Lu, T. B. Nickel complexes as molecular catalysts for water splitting and CO_2 reduction. *Coord. Chem. Rev.* **2019**, *378*, 237−261. (j) Wang, J. W.; Ma, F.; Jin, T.; He,

P.; Luo, Z. M.; Kupfer, S.; Karnahl, M.; Zhao, F.; Xu, Z.; Jin, T.; Lian, T.; Huang, Y. L.; Jiang, L.; Fu, L. Z.; Ouyang, G.; Yi, X. Y. Homoleptic Al(III) Photosensitizers for Durable CO_2 Photoreduction. *J. Am. Chem. Soc.* **2023**, *145*, 676−688. (k) Pugliese, E.; Gotico, P.; Wehrung, I.; Boitrel, B.; Quaranta, A.; Ha-Thi, M. H.; Pino, T.; Sircoglou, M.; Leibl, W.; Halime, Z.; Aukauloo, A. Dissection of Light-Induced Charge Accumulation at a Highly Active Iron Porphyrin: Insights in the Photocatalytic CO_2 Reduction. *Angew. Chem., Int. Ed.* **2022**, *61*, No. e202117530. (l) Peng, L. Y.; Pan, G. N.; Chen, W. K.; Liu, X. Y.; Fang, W. H.; Cui, G. Photocatalytic Reduction of CO_2 to HCOOH and CO by a Phosphine-Bipyridine-Phosphine Ir(III) Catalyst: Photophysics, Nonadiabatic Effects, Mechanism, and Selectivity. *Angew. Chem., Int. Ed.* **2024**, *63*, No. e202315300.

(4) (a) Liang, H. Q.; Beweries, T.; Francke, R.; Beller, M. Molecular Catalysts for the Reductive Homocoupling of CO_2 towards C_{2+} Compounds. *Angew. Chem., Int. Ed.* **2022**, *61*, No. e202200723. (b) Wang, Y. C.; Zhang, J. H.; Yang, W.; Tao, W. X.; Tao, K. Y.; Deng, J. H.; Shi, W. J.; Zhong, D. C.; Lu, T. B. Engineering Coordination Environment of Cobalt Center in Molecular Catalysts for Improved Photocatalytic CO_2 Reduction. *Chin. J. Chem.* **2023**, *41*, 3305−3310.

(5) (a) Ouyang, T.; Huang, H. H.; Wang, J. W.; Zhong, D. C.; Lu, T. B. A Dinuclear Cobalt Cryptate as a Homogeneous Photocatalyst for Highly Selective and Efficient Visible-Light Driven CO_2 Reduction to CO in CH_3CN/H_2O Solution. *Angew. Chem., Int. Ed.* **2017**, *56*, 738−743. (b) Manafe, S. Y.; Le, N.; Lambert, E. C.; Curiac, C.; Nugegoda, D.; Das, S.; Hunt, L. A.; Qu, F.; Whitt, L. M.; Fedin, I.; Hammer, N. I.; Webster, C. E.; Delcamp, J. H.; Papish, E. T. Sensitized and Self-Sensitized Photocatalytic CO_2 Reduction to HCO_2^- and CO under Visible Light with Ni(II) CNC-Pincer Catalysts. *ACS Catal.* **2024**, *14*, 6589−6602.

(6) (a) Fukuzumi, S.; Lee, Y. M.; Ahn, H. S.; Nam, W. Mechanisms of catalytic reduction of CO_2 with heme and nonheme metal complexes. *Chem. Sci.* **2018**, *9*, 6017−6034. (b) Bairagi, A.; Pereverzev, A. Y.; Tinnemans, P.; Pidko, E. A.; Roithová, J. Electrocatalytic CO_2 Reduction: Monitoring of Catalytically Active, Downgraded, and Upgraded Cobalt Complexes. *J. Am. Chem. Soc.* **2024**, *146*, 5480−5492.

(7) (a) Xia, Y. S.; Tang, M.; Zhang, L.; Liu, J.; Jiang, C.; Gao, G. K.; Dong, L. Z.; Xie, L. G.; Lan, Y. Q. Tandem utilization of CO_2 photoreduction products for the carbonylation of aryl iodides. *Nat. Commun.* **2022**, *13*, 2964. (b) Sakakibara, N.; Shizuno, M.; Kanazawa, T.; Kato, K.; Yamakata, A.; Nozawa, S.; Ito, T.; Terashima, K.; Maeda, K.; Tamaki, Y.; Ishitani, O. Surface-Specific Modification of Graphitic Carbon Nitride by Plasma for Enhanced Durability and Selectivity of Photocatalytic CO_2 Reduction with a Supramolecular Photocatalyst. *ACS Appl. Mater. Interfaces* **2023**, *15*, 13205−13218.

(8) (a) Liu, D. C.; Zhong, D. C.; Lu, T. B. Non-noble metal-based molecular complexes for CO_2 reduction: From the ligand design perspective. *EnergyChem.* **2020**, *2*, 100034. (b) Boutin, E.; Merakeb, L.; Ma, B.; Boudy, B.; Wang, M.; Bonin, J.; Anxolabéhère-Mallart, E.; Robert, M. Molecular catalysis of CO_2 reduction: recent advances and perspectives in electrochemical and light-driven processes with selected Fe, Ni and Co aza macrocyclic and polypyridine complexes. *Chem. Soc. Rev.* **2020**, *49*, 5772−5809. (c) An, X.; Tang, Q.; Lan, H.; Liu, H.; Yu, X.; Qu, J.; Lin, H.; Ye, J. Facilitating Molecular Activation and Proton Feeding by Dual Active Sites on Polymeric Carbon Nitride for Efficient CO_2 Photoreduction. *Angew. Chem., Int. Ed.* **2022**, *61*, No. e202212706. (d) Bharti, J.; Chen, L.; Guo, Z.; Cheng, L.; Wellauer, J.; Wenger, O. S.; von Wolff, N.; Lau, K. C.; Lau, T. C.; Chen, G.; Robert, M. Visible-Light-Driven CO_2 Reduction with Homobimetallic Complexes. Cooperativity between Metals and Activation of Different Pathways. *J. Am. Chem. Soc.* **2023**, *145*, 25195−25202.

(9) Thoi, V. S.; Kornienko, N.; Margarit, C. G.; Yang, P.; Chang, C. J. Visible-light photoredox catalysis: selective reduction of carbon dioxide to carbon monoxide by a nickel N-heterocyclic carbene-isoquinoline complex. *J. Am. Chem. Soc.* **2013**, *135*, 14413−14424.

(10) Chen, L.; Guo, Z.; Wei, X. G.; Gallenkamp, C.; Bonin, J.; Anxolabehere Mallart, E.; Lau, K. C.; Lau, T. C.; Robert, M. Molecular Catalysis of the Electrochemical and Photochemical Reduction of CO_2 with Earth-Abundant Metal Complexes. Selective Production of CO vs HCOOH by Switching of the Metal Center. *J. Am. Chem. Soc.* **2015**, *137*, 10918−10921.

(11) (a) Wakabayashi, T.; Kametani, Y.; Tanahashi, E.; Shiota, Y.; Yoshizawa, K.; Jung, J.; Saito, S. Ferrocenyl PNNP Ligands-Controlled Chromium Complex-Catalyzed Photocatalytic Reduction of CO_2 to Formic Acid. *J. Am. Chem. Soc.* **2024**, *146*, 25963−25975. (b) Saito, D.; Yamazaki, Y.; Tamaki, Y.; Ishitani, O. Photocatalysis of a Dinuclear Ru(II)−Re(I) Complex for CO_2 Reduction on a Solid Surface. *J. Am. Chem. Soc.* **2020**, *142*, 19249−19258. (c) Li, N.-X.; Chen, Y.-M.; Xu, Q.-Q.; Mu, W.-H. Photocatalytic reduction of CO_2 to CO using nickel(II)-bipyridine complexes with different substituent groups as catalysts. *Journal of CO_2 Utilization* **2023**, *68*, 102385.

(12) (a) Liu, D. C.; Zhang, M. L.; Huang, H. H.; Feng, Q.; Su, C.; Mo, A. N.; Wang, J. W.; Qi, Z. P.; Zhang, X. J.; Jiang, L.; Chen, Z. L. Co^{II}−Zn^{II} Heterometallic Dinuclear Complex with Enhanced Photocatalytic Activity for CO_2-to-CO Conversion in a Water-Containing System. *ACS Sustain. Chem. Eng.* **2021**, *9*, 9273−9281. (b) Su, C.; Chen, Z.; Feng, Q.; Wei, F.; Mo, A.; Huang, H. H.; Hu, H.; Zou, H.; Liang, F.; Liu, D. Electronic effects promoted the catalytic activities of binuclear $Co_{(II)}$ complexes for visible-light-driven CO_2 reduction in a water-containing system. *Dalton Trans.* **2023**, *52*, 4548−4553.

(13) (a) Cheung, P. L.; Machan, C. W.; Malkhasian, A. Y.; Agarwal, J.; Kubiak, C. P. Photocatalytic Reduction of Carbon Dioxide to CO and HCO_2H Using fac-Mn(CN)(bpy)$(CO)_3$. *Inorg. Chem.* **2016**, *55*, 3192−3198. (b) Fei, H.; Sampson, M. D.; Lee, Y.; Kubiak, C. P.; Cohen, S. M. Photocatalytic CO_2 Reduction to Formate Using a Mn(I) Molecular Catalyst in a Robust Metal-Organic Framework. *Inorg. Chem.* **2015**, *54*, 6821−6828. (c) Guo, Z.; Cheng, S.; Cometto, C.; Anxolabehere-Mallart, E.; Ng, S. M.; Ko, C. C.; Liu, G.; Chen, L.; Robert, M.; Lau, T. C. Highly Efficient and Selective Photocatalytic CO_2 Reduction by Iron and Cobalt Quaterpyridine Complexes. *J. Am. Chem. Soc.* **2016**, *138*, 9413−9416. (d) Shimoda, T.; Morishima, T.; Kodama, K.; Hirose, T.; Polyansky, D. E.; Manbeck, G. F.; Muckerman, J. T.; Fujita, E. Photocatalytic CO_2 Reduction by Trigonal-Bipyramidal Cobalt(II) Polypyridyl Complexes: The Nature of Cobalt(I) and Cobalt(0) Complexes upon Their Reactions with CO_2, CO, or Proton. *Inorg. Chem.* **2018**, *57*, 5486−5498.

(14) (a) Hong, D.; Tsukakoshi, Y.; Kotani, H.; Ishizuka, T.; Kojima, T. Visible-Light-Driven Photocatalytic CO_2 Reduction by a Ni(II) Complex Bearing a Bioinspired Tetradentate Ligand for Selective CO Production. *J. Am. Chem. Soc.* **2017**, *139*, 6538−6541. (b) Xiao, Y.; Xie, F.; Zhang, H.-T.; Zhang, M.-T. Bioinspired Binickel Catalyst for Carbon Dioxide Reduction: The Importance of Metal−ligand Cooperation. *JACS Au* **2024**, *4*, 1207−1218.

(15) (a) Liu, D. C.; Luo, Z. M.; Aramburu-Trošelj, B. M.; Fan, M.; Wang, J. W. Cobalt-based tripodal complexes as molecular catalysts for photocatalytic CO_2 reduction. *Chem. Commun.* **2023**, *59*, 14626−14635. (b) Feng, Q.; Huang, C. Z.; Chen, Z. l.; Huang, Z. B.; Huang, H. H.; Hu, H. C.; Liang, F. P.; Liu, D. C. Electronic Effect Promoted Visible-Light-Driven CO_2-to-CO Conversion in a Water-Containing System. *Inorg. Chem.* **2023**, *62*, 21416−21423.

(16) (a) Lee, S. E.; Nasirian, A.; Kim, Y. E.; Fard, P. T.; Kim, Y.; Jeong, B.; Kim, S. J.; Baeg, J. O.; Kim, J. Visible-Light Photocatalytic Conversion of Carbon Dioxide by Ni(II) Complexes with N4S2 Coordination: Highly Efficient and Selective Production of Formate. *J. Am. Chem. Soc.* **2020**, *142*, 19142−19149. (b) Fogeron, T.; Retailleau, P.; Gomez-Mingot, M.; Li, Y.; Fontecave, M. Nickel Complexes Based on Molybdopterin-like Dithiolenes: Catalysts for CO_2 Electroreduction. *Organometallics* **2019**, *38*, 1344−1350. (c) Fogeron, T.; Todorova, T. K.; Porcher, J. P.; Gomez-Mingot, M.; Chamoreau, L. M.; Mellot Draznieks, C.; Li, Y.; Fontecave, M. A Bioinspired Nickel(bis-dithiolene) Complex as a Homogeneous Catalyst for Carbon Dioxide Electroreduction. *ACS Catal.* **2018**, *8*, 2030−2038. (d) Hong, D.; Kawanishi, T.; Tsukakoshi, Y.; Kotani, H.;

https://doi.org/10.1021/acscatal.4c04800
ACS Catal. 2025, 15, 2522−2530

Ishizuka, T.; Kojima, T. Efficient Photocatalytic CO_2 Reduction by a Ni(II) Complex Having Pyridine Pendants through Capturing a Mg^{2+} Ion as a Lewis-Acid Cocatalyst. *J. Am. Chem. Soc.* **2019**, *141*, 20309−20317.

(17) Torelli, S.; Orio, M.; Pecaut, J.; Jamet, H.; Le Pape, L.; Menage, S. A $\{Cu_2S\}^{2+}$ Mixed-Valent Core Featuring a Cu-Cu Bond. *Angew. Chem., Int. Ed.* **2010**, *49*, 8249−8252.

(18) (a) Platzman, I.; Brener, R.; Haick, H.; Tannenbaum, R. Oxidation of Polycrystalline Copper Thin Films at Ambient Conditions. *J. Phys. Chem. C* **2008**, *112*, 1101−1108. (b) Wang, Y.; Zhou, W.; Jia, R.; Yu, Y.; Zhang, B. Unveiling the Activity Origin of a Copper-based Electrocatalyst for Selective Nitrate Reduction to Ammonia. *Angew. Chem., Int. Ed.* **2020**, *59*, 5350−5354. (c) Hu, F.; Yang, L.; Jiang, Y.; Duan, C.; Wang, X.; Zeng, L.; Lv, X.; Duan, D.; Liu, Q.; Kong, T.; Jiang, J.; Long, R.; Xiong, Y. Ultrastable Cu Catalyst for CO_2 Electroreduction to Multicarbon Liquid Fuels by Tuning C-C Coupling with CuTi Subsurface. *Angew. Chem., Int. Ed.* **2021**, *60*, 26122−26127.

(19) (a) Ziegler, M. S.; Levine, D. S.; Lakshmi, K. V.; Tilley, T. D. Aryl Group Transfer from Tetraarylborato Anions to an Electrophilic Dicopper(I) Center and Mixed-Valence mu-Aryl Dicopper(I,II) Complexes. *J. Am. Chem. Soc.* **2016**, *138*, 6484−6491. (b) Gagne, R. R.; Koval, C. A.; Smith, T. J.; Cimolino, M. C. Binuclear Complexes of Macrocyclic Ligands. Electrochemical and Spectral Properties of Homobinuclear $Cu^{II}Cu^{II}$, $Cu^{II}Cu^{I}$, and $Cu^{I}Cu^{I}$ Species Including an Estimated Intramolecular Electron Transfer Rate. *J. Am. Chem. Soc.* **1979**, *101*, 4571−4580. (c) Long, R. C.; Hendrickson, D. N. Intramolecular Electron Transfer in a Series of Mixed-Valence Copper(II)-Copper(I) Complexes. *J. Am. Chem. Soc.* **1983**, *105*, 1513−1521.

(20) Craig, C. A.; Spreer, L. O.; Otvos, J. W.; Calvin, M. Photochemical Reduction of Carbon Dioxide Using Nickel Tetraazamacrocycles. *J. Phys. Chem.* **1990**, *94*, 7957−7960.

(21) Ouyang, T.; Wang, H.-J.; Huang, H.-H.; Wang, J.-W.; Guo, S.; Liu, W.-J.; Zhong, D.-C.; Lu, T.-B. Dinuclear Metal Synergistic Catalysis Boosts Photochemical CO_2-to-CO Conversion. *Angew. Chem. Int. Ed* **2018**, *57*, 16480−16485.

(22) (a) Gong, Y.-N.; Mei, J.-H.; Shi, W.-J.; Liu, J.-W.; Zhong, D.-C.; Lu, T.-B. Boosting CO_2 Photoreduction to Formate or CO with High Selectivity over a Covalent Organic Framework Covalently Anchored on Graphene Oxide. *Angew. Chem., Int. Ed.* **2024**, *63*, No. e202318735. (b) Xu, H.-Q.; Hu, J.; Wang, D.; Li, Z.; Zhang, Q.; Luo, Y.; Yu, S.-H.; Jiang, H.-L. Visible-Light Photoreduction of CO_2 in a Metal−Organic Framework: Boosting Electron−Hole Separation via Electron Trap States. *J. Am. Chem. Soc.* **2015**, *137*, 13440−13443.

(23) (a) Matsuoka, S.; Yamamoto, K.; Ogata, T.; Kusaba, M.; Nakashima, N.; Fujita, E.; Yanagida, S. Efficient and selective electron mediation of cobalt complexes with cyclam and related macrocycles in the p-terphenyl-catalyzed photoreduction of carbon dioxide. *J. Am. Chem. Soc.* **1993**, *115*, 601−609. (b) Takeda, H.; Koizumi, H.; Okamoto, K.; Ishitani, O. Photocatalytic CO_2 reduction using a Mn complex as a catalyst. *Chem. Commun.* **2014**, *50*, 1491−1493.

(24) Takeda, H.; Kamiyama, H.; Okamoto, K.; Irimajiri, M.; Mizutani, T.; Koike, K.; Sekine, A.; Ishitani, O. Highly Efficient and Robust Photocatalytic Systems for CO_2 Reduction Consisting of a Cu(I) Photosensitizer and Mn(I) Catalysts. *J. Am. Chem. Soc.* **2018**, *140*, 17241−17254.

(25) (a) Bharti, J.; Chen, L.; Guo, Z.; Cheng, L.; Wellauer, J.; Wenger, O. S.; von Wolff, N.; Lau, K.-C.; Lau, T.-C.; Chen, G.; Robert, M. Visible-Light-Driven CO_2 Reduction with Homobimetallic Complexes. Cooperativity between Metals and Activation of Different Pathways. *J. Am. Chem. Soc.* **2023**, *145*, 25195−25202. (b) Guo, Z.; Yu, F.; Yang, Y.; Leung, C.-F.; Ng, S.-M.; Ko, C.-C.; Cometto, C.; Lau, T.-C.; Robert, M. Photocatalytic Conversion of CO_2 to CO by a Copper(II) Quaterpyridine Complex. *ChemSusChem* **2017**, *10*, 4009−4013.

(26) (a) Chan, S. L.; Lam, T. L.; Yang, C.; Yan, S. C.; Cheng, N. M. A robust and efficient cobalt molecular catalyst for CO_2 reduction. *Chem. Commun.* **2015**, *51*, 7799−7801. (b) Zhao, J. S.; Mu, Y. F.; Wu, L. Y.; Luo, Z. M.; Velasco, L.; Sauvan, M.; Moonshiram, D.; Wang, J. W.; Zhang, M.; Lu, T. B. Directed Electron Delivery from a Pb-Free Halide Perovskite to a Co(II) Molecular Catalyst Boosts CO_2 Photoreduction Coupled with Water Oxidation. *Angew. Chem., Int. Ed.* **2024**, *63*, No. e202401344.

(27) (a) Zall, C. M.; Linehan, J. C.; Appel, A. M. Triphosphine-Ligated Copper Hydrides for CO_2 Hydrogenation: Structure, Reactivity, and Thermodynamic Studies. *J. Am. Chem. Soc.* **2016**, *138*, 9968−9977. (b) Aloisi, A.; Crochet, E.; Nicolas, E.; Berthet, J.-C.; Lescot, C.; Thuéry, P.; Cantat, T. Copper−Ligand Cooperativity in H_2 Activation Enables the Synthesis of Copper Hydride Complexes. *Organometallics* **2021**, *40*, 2064−2069.

(28) Gong, Y.-N.; Zhong, W.; Li, Y.; Qiu, Y.; Zheng, L.; Jiang, J.; Jiang, H.-L. Regulating Photocatalysis by Spin-State Manipulation of Cobalt in Covalent Organic Frameworks. *J. Am. Chem. Soc.* **2020**, *142*, 16723−16731.

https://doi.org/10.1021/acscatal.4c04800
ACS Catal. 2025, 15, 2522−2530